

Evolutionary Benefits of Fitness-Dependent Mutation Rates

Andrew G. T. Pyo¹, Qiwei Yu², Julia Merckenschlager³, and Ned S. Wingreen^{2,4,*}

¹*Department of Physics, Princeton University, Princeton, New Jersey 08544, USA*

²*Lewis-Sigler Institute for Integrative Genomics, Princeton University, Princeton, New Jersey 08544, USA*

³*Department of Immunology, Harvard Medical School, Boston, Massachusetts 02115, USA*

⁴*Department of Molecular Biology, Princeton University, Princeton, New Jersey 08544, USA*

 (Received 15 December 2024; revised 25 March 2025; accepted 17 June 2025; published 24 July 2025)

Motivated by recent observations that mutation rates can be correlated with individual fitness, we analyze an evolutionary hill-climbing model with fitness-dependent mutation rates. Our results show that a mutation rate that decreases with increasing relative fitness can greatly accelerate the accumulation of beneficial mutations. Moreover, we show that a lower mutation rate for fitter individuals can prevent “mutational meltdown” of small populations by decreasing the probability of fixation of deleterious mutations. These findings suggest potential strategies for accelerating the adaptation of populations to environmental changes.

DOI: 10.1103/szpk-sx1c

Diversification through random mutation is a fundamental driving force for evolution in living systems. The rate at which a population adapts is governed by the variation in fitness within the population, which arises from a balance between opposing forces—mutation and selection [1–3]. Typically, mutation rates are assumed to be constant across the population. However, recent findings show that B cells expressing high-affinity antibodies experience a reduced mutation rate per division through modulating their time spent in G0/G1 [4,5]. Mechanistically, dynamic mutation rates in B cells are regulated by T cells, which provide help signals proportional to B cell affinity, thereby instructing for the number and speed of B cell divisions [6]. Faster B cell division acts to shorten time spent in G0/G1 phases, which limits exposure of the genome to the mutagenic enzyme activation-induced cytidine deaminase [7], and effectively lowering the per-division mutation rate for higher-affinity B cells over the course of a proliferative burst (approximately six divisions for high-affinity B cells).

Outside of affinity maturation, correlations between mutation rate and fitness have been observed in a variety of systems, including RNA viruses and *Escherichia coli*, with both positive and negative correlations reported [8–10]. Motivated by these findings, we set out to understand how fitness-mutation rate correlations

could influence population evolution and whether they can confer evolutionary advantages.

Numerous studies have characterized the role of selection, mutation, and population size on the adaptation of asexual populations [11–17]. However, the case of within-population fitness-dependent mutation rates has been mostly limited to binary mutator or nonmutator cases [18–20]. To examine how more general fitness-dependent mutation rates influence the evolution of an asexual population, we consider a simple birth-death process with mutations [21].

Here, we characterize each individual by their heritable phenotype (e.g., antibody affinity for B cells), which we classify with a discrete coordinate x_n that corresponds with a birth rate, aka “fitness,” $B_n(t)$ [22,23]. Without loss of generality, we order x_n such that $B_n(t)$ is a monotonically increasing function of n . Upon each birth event, a non-neutral mutation occurs with phenotype-dependent probability $p_n(t)$, and these cause a change in the new individual’s phenotype and thus its fitness [Fig. 1(a)]. To maintain the average population size of $N = \sum_n N_n$, where N_n is the number of individuals with phenotype x_n , we set a global death rate proportional to the population’s average fitness. To systematically expand in the terms of the population size, we let $N_n = N\varphi_n + \sqrt{N}\xi_n$, where φ_n is the mean-field population density and ξ_n represents demographic noise [24]. The mean-field dynamics can be derived from the corresponding master equation as (see the Appendix)

$$\partial_t \varphi_n(t) = [B_n(t) - \langle B_n \rangle(t)] \varphi_n(t) + \mathcal{J}_n(t), \quad (1)$$

where $\langle f_n \rangle(t) = \sum_n \varphi_n(t) f_n$, and \mathcal{J}_n is the flux due to mutations. \mathcal{J}_n determines the net flux of individuals into each phenotype due to mutations, and can be written as

*Contact author: wingreen@princeton.edu

Published by the American Physical Society under the terms of the Creative Commons Attribution 4.0 International license. Further distribution of this work must maintain attribution to the author(s) and the published article’s title, journal citation, and DOI.

$$\mathcal{J}_n(t) = -H_n(t) + \sum_{m \neq n} K_{n-m} H_m(t), \quad (2)$$

where K_{n-m} is the normalized mutation kernel representing the probability that a mutation induces a change from phenotype x_m to x_n , and $H_n(t) = p_n(t) B_n(t) \varphi_n(t)$ is the density outflux from x_n due to mutations. Note that in the mean-field dynamics, finite population size is accounted for by setting $B_n(t) = 0$ if $\varphi_n(t) < 1/N$ [25].

From Eq. (1), an expression for the adaptation velocity $v(t) \equiv d\langle n \rangle / dt$ can be obtained by multiplying by n and integrating

$$v(t) = C_{n,B}(t) + \mu_K \langle B_n p_n \rangle(t), \quad (3)$$

where $C_{n,B}(t) = \langle n B_n \rangle - \langle n \rangle \langle B_n \rangle$ is the covariance function, and $\mu_K = \sum_{\Delta n} \Delta n K_{\Delta n}$ is the first moment of the mutation kernel which characterizes the average effect of mutations.

The first term in Eq. (3) represents the contribution from selection, while the second term accounts for mutations. Since most non-neutral mutations are deleterious (reduce fitness), this implies $\mu_K < 0$. As a result, a negative correlation between B_n and p_n , indicating that fitter individuals have a lower mutation probability per division, maximizes v .

To gain further intuition, we consider a simple mutation model where a certain fraction γ_b of mutations are beneficial, with each increasing n by unity ($n \rightarrow n + 1$), and a fraction $1 - \gamma_b$ are deleterious ($n \rightarrow n - 1$). Furthermore, we limit B_n and p_n to be linear functions of relative fitness, i.e.,

$$B_n(t) = B_0 + s[n - \langle n \rangle(t)], \quad (4a)$$

$$p_n(t) = P_0 + (\eta/s)[B_n(t) - \langle B_n \rangle(t)]. \quad (4b)$$

Here, $B_0 = 1$ (set to unity by choosing an appropriate unit of time) is the average birth rate of the population, $s > 0$ is the fitness gain/loss due to a mutation, P_0 is the average mutation probability at each birth event, and η gives the slope of the mutation probability as a function of fitness. In this case, the expression for v [Eq. (3)] simplifies to

$$v(t) = s(1 + \mu_K \eta) \sigma^2(t) + \mu_K P_0 B_0, \quad (5)$$

where $\sigma^2 = \langle n^2 \rangle - \langle n \rangle^2$ is the phenotypic variance in the population, and $\mu_K = 2\gamma_b - 1$.

As seen in Eq. (6), the speed of adaptation v is influenced by η . For a modest population size of $N = 10^4$, and when most mutations are deleterious ($\gamma_b = 0.05$), a uniform mutation probability ($\eta = 0$) results in a slow, or even negative adaptation speed due to the high probability of each mutation being deleterious [see Fig. 1(b)]. On the other hand, a mutation probability that decreases with

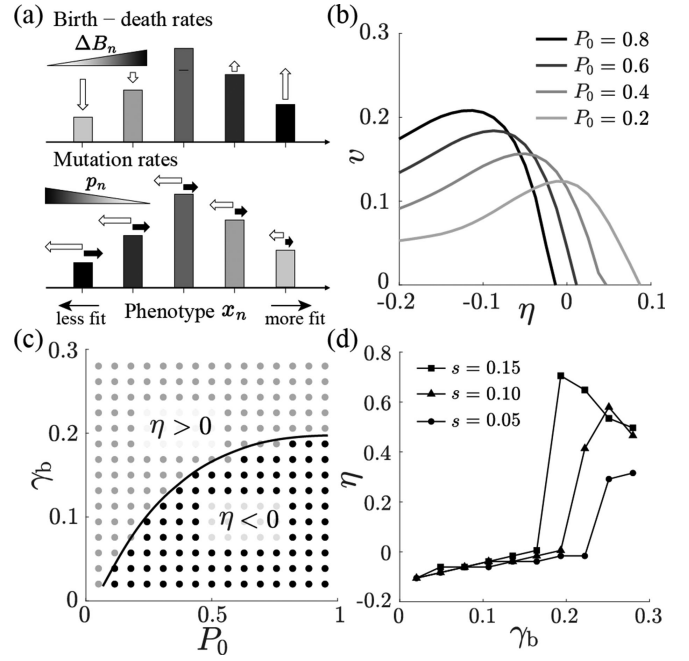


FIG. 1. (a) Schematic of the birth-death-mutation process along a phenotype coordinate. (b) Adaptation speed v shown as a function of the slope in mutation probability η , for several values of the average mutation probability P_0 . (c) “Phase diagram” illustrating the sign of η that maximizes v ; solid curve shows the boundary as a guide to the eye. (d) Optimal η as a function of the fraction of beneficial mutation γ_b , for different values of fitness change per mutation s . Unless otherwise specified, simulation parameters were $\gamma_b = 0.05$, $s = 0.15$, and $N = 10^4$. For (b)–(d), simulation of the mean-field dynamics (see Supplemental Material [26]) was done with $\Delta t = 0.001$ (in unit of B_0^{-1}).

relative fitness ($\eta < 0$) maximizes the adaptation speed v . Interestingly, whether a decreasing or an increasing fitness-dependent mutation rate is best for adaptation depends on P_0 and γ_b . As shown in Fig. 1(c), we find that $\eta < 0$ is optimal when mutations are frequent (large P_0) but rarely beneficial (small γ_b), which is the case, e.g., in B cell (antibody) affinity maturation [18]. Conversely, if deleterious mutations occur less frequently (due either to small P_0 or large γ_b), $\eta > 0$ becomes optimal, as further described below.

The value of η that maximizes v undergoes a strikingly rapid transition as the “phase boundary” in Fig. 1(c) is crossed. As shown in Fig. 1(d), the optimal η is negative for small γ_b , but dramatically increases to a positive value for larger γ_b . This jump in η reflects a shift in the optimal adaptation strategy from a *selection driven* mechanism at small γ_b , to a *flux driven* mechanism at larger γ_b . These two mechanisms can be understood heuristically as follows: From a system-size expansion of the master equation, the mean-field dynamics and the demographic noise of the current fittest individuals, aka the “nose” of the population, are given by

$$\partial_t \varphi_{n^*} = r_{n^*} \varphi_{n^*} + \gamma_b J_{n^*}, \quad (6a)$$

$$\partial_t \langle \xi_{n^*}^2 \rangle_{\Pi} = 2r_{n^*} \langle \xi_{n^*}^2 \rangle_{\Pi} + \rho_{n^*} \varphi_{n^*} + \gamma_b \dot{J}_{n^*}, \quad (6b)$$

where x_{n^*} denotes the nose phenotype, $r_n = (1 - p_n)B_n - \langle B_n \rangle$ and $\rho_n = (1 + p_n)B_n + \langle B_n \rangle$ are the effective Malthusian growth parameters, and J_{n^*} and \dot{J}_{n^*} are mutational source terms (see the Appendix).

Assuming the mutation fluxes J_{n^*} and \dot{J}_{n^*} remain approximately constant during the establishment of the nose, Eqs. (6a) and (6b) reveal two distinct mechanisms of adaptive hill climbing, depending on the sign of r_{n^*} : (i) *Selection driven hill climbing* ($r_{n^*} > 0$, i.e., $p_{n^*} < 1 - B_0/B_{n^*}$)—When mutations at the nose are rare, net nose population growth due to birth events dominates over mutation flux, leading to exponential growth of the nose population, with corresponding demographic noise ($\varphi_{n^*} \sim e^{r_{n^*} t}$, and $\langle \xi_{n^*}^2 \rangle_{\Pi} \sim \varphi_{n^*}^2$). In this case, establishment of the nose is reliant on preferential birth events conferred by the nose’s fitness advantage. (ii) *Flux driven hill climbing* ($r_{n^*} < 0$, i.e., $p_{n^*} > 1 - B_0/B_{n^*}$)—Alternatively, the nose population can be stabilized by sufficient density influx via beneficial mutations from phenotype x_{n^*-1} , leading to fixed point $\bar{\varphi}_{n^*} = \gamma_b J_{n^*} / |r_{n^*}|$ with $\bar{\xi}_{n^*}^2 = (\rho_{n^*} \varphi_{n^*} + \gamma_b \dot{J}_{n^*}) / 2|r_{n^*}|$.

This distinction naturally leads to the question: how might η be adjusted to ensure the optimal hill-climbing strategy? When beneficial mutations are rare (small γ_b), the mutation flux alone is too small to stabilize the nose population. Thus, exponential growth through a selection driven mechanism (via small mutation probability p_{n^*} corresponding to $\eta < 0$) is needed for optimal adaptation. Conversely, when beneficial mutations are frequent (large γ_b), the flux driven mechanism (with larger p_{n^*} , corresponding to $\eta > 0$) leads to a sufficiently large stable nose population capable of propagating new fittest mutants. For these reasons, the optimal value of η is strongly dependent on both γ_b and P_0 .

In the biologically relevant regime where beneficial mutations are rare, what determines the optimal value of η ? To answer this question, we utilized an agent-based simulation, where we could explicitly take into account the stochasticity of the nose population (see Supplemental Material [26]). Using the agent-based simulation, we found that for the selection driven mechanism, the impact of the mutation-fitness correlation embodied by η on the dynamics of the fittest individuals reflects a tradeoff between two key timescales: an “entrenchment time” τ_{ent} , which reflects the time required for the nose to overcome drift-driven extinction, and τ_{new} , the typical time it takes an entrenched nose population to acquire a positive, beneficial mutation, thereby generating a new fittest individual, i.e., a new “nose” (see Fig. 2, inset).

Intuitively, when beneficial mutations are rare, τ_{ent} increases with η , as a higher mutation rate at the nose

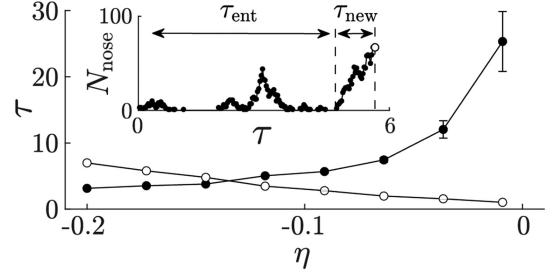


FIG. 2. Average time spent attempting to entrench the fittest (nose) population τ_{ent} (solid circles), and the average time required to generate the new fittest individual τ_{new} (empty circles) shown as a function of η . Agent-based simulations (see Supplemental Material [26]) were used with parameters $s = 0.15$, $N = 10^4$, $P_0 = 0.5$, $\gamma_b = 0.05$, $\Delta t = 0.003$. Error bars represent the standard error over 10 simulation runs. Inset: example of a time trajectory of the number of fittest individuals N_{nose} . Following multiple extinction events, the nose becomes entrenched; the empty circle represents the point where a new nose is first generated.

results in frequent acquisition of deleterious mutations, which promotes extinction (Fig. 2, solid circles). Conversely, increasing η expedites the appearance of the next fittest individual by increasing the mutation rate at the nose, thus increasing the chances of acquiring a beneficial mutation and decreasing τ_{new} (Fig. 2, empty circles). Thus, optimizing the speed of adaptation requires balancing the two timescales τ_{ent} and τ_{new} .

The speed of adaptation is not the only consideration in evolving populations. For example, deleterious mutations can often fix in asexual populations due to lack of recombination. Continued accumulation of deleterious mutations can then lead to declining fitness of the whole population ultimately leading to extinction by “mutational meltdown” [27,28]. As η has a strong influence on the mutational dynamics, we wondered whether a nonzero η could mitigate mutational meltdown.

In selecting the functional form of fitness [Eq. (4a)], we assumed a competitive regime where the average birth rate remains fixed at B_0 , with population size controlled by a global death rate, ensuring no overall extinction. Despite this simplification, the model can still provide insights into the population-level accumulation rates of beneficial and deleterious mutations. The speed of adaptation can be understood as the net difference between the average per-cell rates of accumulation for beneficial and deleterious mutations, denoted \dot{m}_+ and \dot{m}_- (i.e., $v = \dot{m}_+ - \dot{m}_-$).

Using agent-based simulations to individually track the accumulation of beneficial and deleterious mutations, we observe that the accumulation rate of beneficial mutations \dot{m}_+ [Fig. 3(a), solid circles] remains relatively constant and symmetric with respect to η . In contrast, the accumulation rate of deleterious mutations \dot{m}_- [Fig. 3(a), empty circles] is significantly slower for $\eta < 0$, nearly vanishing at sufficiently negative η values. Thus, a mutation probability

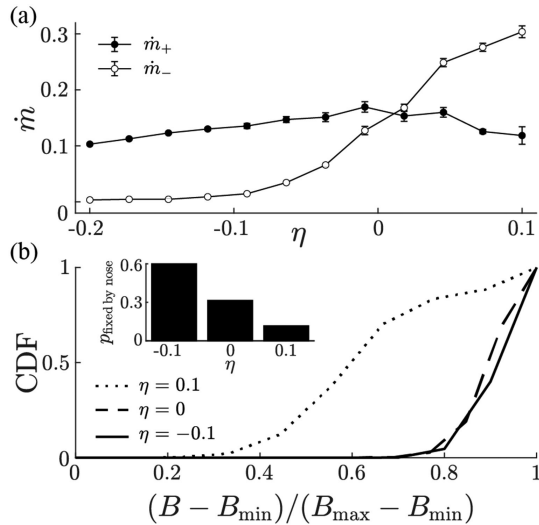


FIG. 3. (a) Rates of change of the average number of beneficial mutations (\dot{m}_+) and deleterious mutations (\dot{m}_-) in the population as functions of η . Error bars represent the standard error over 10 simulation runs. (b) Cumulative distribution function (CDF) p_{fixed} as a function of scaled, relative fitness for different values of η . Inset: probability that a fixation event originated from an individual at the nose ($p_{\text{fixed by nose}}$). In (a),(b) agent-based simulations (see Supplemental Material [26]) were performed with parameters $s = 0.1$, $\gamma_b = 0.05$, $N = 10^4$, and $\Delta t = 0.003$.

that decreases with relative fitness can effectively prevent the buildup of deleterious mutations, while maintaining the accumulation rate of beneficial mutations.

Intuitively, how η influences the accumulation of deleterious mutations can be illustrated as follows. As discussed above, when $\eta > 0$, there is a sufficient flux of beneficial mutations to enable initially unfit individuals to “swim upstream” and end up at the nose, where they have the potential to become fixed (ancestral to the entire population). In this case, their deleterious mutations will also be permanently fixed in the population. Conversely, when $\eta < 0$, the mutation-driven loss of fitness among unfit individuals is accelerated, leading to their elimination from the population by selection. Thus, $\eta < 0$ creates a system in which fitter individuals are shielded from deleterious mutations, while unfit individuals are quickly “purged,” reducing the overall rate of accumulation of deleterious mutations by the population.

This purging effect is illustrated in Fig. 3(b), which shows that when $\eta = -0.1$, only the individuals at the nose of the population’s fitness distribution have the potential to become fixed. In contrast, when $\eta = 0.1$, individuals with lower relative fitness also have a chance of fixation. Notably, we observe an approximately sixfold increase in $p_{\text{fixed by nose}}$, the probability that a fixation event originated from an individual at the nose, when $\eta = -0.1$ compared to when $\eta = 0.1$ [see Fig. 3(b), inset]. In a nutshell, a negative η preferentially stabilizes high-fitness

individuals, enhancing the likelihood of fixation among the fittest members, which typically have the fewest deleterious mutations, and this reduces the accumulation of deleterious mutations in the population.

Mutation rates are subject to selection, and correlations between fitness and mutation rates have been observed across multiple biological systems [8–10]. Whether this relationship arises from biological constraints, such as low-fitness individuals being unable to allocate resources for high-fidelity reproduction, or from evolutionary optimization remains unclear. Nonetheless, in this Letter, we demonstrated that such a correlation can confer significant evolutionary benefits, particularly when beneficial mutations are rare, a scenario common in biology [29]. Specifically, fitness-dependent mutation rates can accelerate adaptation and reduce the fixation of deleterious mutations. In the case of a well-defined fitness maximum, a negative η will enhance the stability of the quasi-species localized around the maximum [30].

These advantages are particularly relevant in systems requiring rapid adaptation, such as the adaptive immune system, where B cells must evolve quickly to produce increasingly high-affinity antibodies to bind and neutralize pathogens—a process that can occur over weeks to months [31]. Similarly, in asexual populations, fitness-dependent mutation rates may mitigate the risk of mutational meltdown, a critical factor in population extinction. This effect becomes more significant the more loci there are for deleterious mutations. Beyond natural systems, our findings have implications for improving evolutionary algorithms [32] and directed evolution [33], which are widely used to optimize complex systems, such as identifying proteins with desired characteristics [34]. Incorporating fitness-dependent mutation rates into these frameworks could optimize search strategies based on the fitness landscape and the primary objective, such as maximizing speed or minimizing unnecessary steps. This approach could improve processes like particle swarm optimization [35] by tuning the exploration and exploitation balance through fitness-dependent mutation rates. In directed evolution, decreasing mutation rates based on functional output could prevent unnecessary mutations in fit variants, thereby maintaining structural stability—addressing a common challenge in protein engineering [36].

Finally, investigating the implications of fitness-dependent mutation rates beyond the simple hill-climbing model presented here could be fruitful for understanding the long-term stability and adaptive potential of both natural and engineered systems.

Acknowledgments—This work was supported in part by the Natural Sciences and Engineering Research Council of Canada (A. G. T. P), Harold W. Dodds Fellowship (Q. Y.), Branco Weiss Fellowship (J. M.), and in part by the

National Science Foundation, through the Center for the Physics of Biological Function (PHY-1734030). The authors acknowledge Matthew E. Black for critical reading of the manuscript, and Michel C. Nussenzweig for helpful discussions.

Data availability—The data that support the findings of this Letter are openly available [37].

-
- [1] J. Haigh, The accumulation of deleterious genes in a population—Muller’s Ratchet, *Theor. Popul. Biol.* **14**, 251 (1978).
- [2] M. Lynch, M. S. Ackerman, J.-F. Gout, H. Long, W. Sung, W. K. Thomas, and P. L. Foster, Genetic drift, selection and the evolution of the mutation rate, *Nat. Rev. Genet.* **17**, 704 (2016).
- [3] M. M. Desai and D. S. Fisher, Beneficial mutation–selection balance and the effect of linkage on positive selection, *Genetics* **176**, 1759 (2007).
- [4] J. Merckenschlager, A. G. T. Pyo, G. S. Silva Santos, D. Schaefer-Babajew, M. Cipolla, H. Hartweger, A. D. Gitlin, N. S. Wingreen, and M. C. Nussenzweig, Regulated somatic hypermutation enhances antibody affinity maturation, *Nature (London)* **641**, 495 (2025).
- [5] J. Pae *et al.*, Transient silencing of hypermutation preserves B cell affinity during clonal bursting, *Nature (London)* **641**, 486 (2025).
- [6] A. D. Gitlin, C. T. Mayer, T. Y. Oliveira, Z. Shulman, M. J. K. Jones, A. Koren, and M. C. Nussenzweig, T cell help controls the speed of the cell cycle in germinal center B cells, *Science* **349**, 643 (2015).
- [7] J. S. Rush, M. Liu, V. H. Odegard, S. Unniraman, and D. G. Schatz, Expression of activation-induced cytidine deaminase is regulated by cell division, providing a mechanistic basis for division-linked class switch recombination, *Proc. Natl. Acad. Sci. U.S.A.* **102**, 13242 (2005).
- [8] Z. Lao, Y. Matsui, S. Ijichi, and B.-W. Ying, Global coordination of the mutation and growth rates across the genetic and nutritional variety in *Escherichia coli*, *Front. Microbiol.* **13**, 990969 (2022).
- [9] K. Husain, V. Sachdeva, R. Ravasio, M. Peruzzo, W. Liu, B. H. Good, and A. Murugan, Direct and indirect selection in a proofreading polymerase, *bioArXiv* (2025), [10.1101/2024.10.14.618309](https://doi.org/10.1101/2024.10.14.618309).
- [10] V. Furió, A. Moya, and R. Sanjuán, The cost of replication fidelity in an RNA virus, *Proc. Natl. Acad. Sci. U.S.A.* **102**, 10233 (2005).
- [11] J. Marchi, M. Lässig, A. M. Walczak, and T. Mora, Antigenic waves of virus–immune coevolution, *Proc. Natl. Acad. Sci. U.S.A.* **118**, e2103398118 (2021).
- [12] O. Hallatschek, The noisy edge of traveling waves, *Proc. Natl. Acad. Sci. U.S.A.* **108**, 1783 (2011).
- [13] R. Servajean and A.-F. Bitbol, Impact of population size on early adaptation in rugged fitness landscapes, *Phil. Trans. R. Soc. B* **378**, 20220045 (2023).
- [14] C. K. Fisher and P. Mehta, The transition between the niche and neutral regimes in ecology, *Proc. Natl. Acad. Sci. U.S.A.* **111**, 13111 (2014).
- [15] B. H. Good, I. M. Rouzine, D. J. Balick, O. Hallatschek, and M. M. Desai, Distribution of fixed beneficial mutations and the rate of adaptation in asexual populations, *Proc. Natl. Acad. Sci. U.S.A.* **109**, 4950 (2012).
- [16] B. H. Good and M. M. Desai, Evolution of mutation rates in rapidly adapting asexual populations, *Genetics* **204**, 1249 (2016).
- [17] J. T. Ferrare and B. H. Good, Evolution of evolvability in rapidly adapting populations, *Nat. Ecol. Evol.* **8**, 2085 (2024).
- [18] M. M. Desai and D. S. Fisher, The balance between mutators and nonmutators in asexual populations, *Genetics* **188**, 997 (2011).
- [19] Y. Ram and L. Hadany, The evolution of stress-induced hypermutation in asexual populations, *Evolution* **66**, 2315 (2012).
- [20] Y. Ram and L. Hadany, Stress-induced mutagenesis and complex adaptation, *Proc. R. Soc. B* **281**, 20141025 (2014).
- [21] S. Goyal, D. J. Balick, E. R. Jerison, R. A. Neher, B. I. Shraiman, and M. M. Desai, Dynamic mutation–selection balance as an evolutionary attractor, *Genetics* **191**, 1309 (2012).
- [22] T. B. Kepler and A. S. Perelson, Cyclic re-entry of germinal center B cells and the efficiency of affinity maturation, *Immunol. Today* **14**, 412 (1993).
- [23] G. Chure, M. Razo-Mejia, N. M. Belliveau, T. Einav, Z. A. Kaczmarek, S. L. Barnes, M. Lewis, and R. Phillips, Predictive shifts in free energy couple mutations to their phenotypic consequences, *Proc. Natl. Acad. Sci. U.S.A.* **116**, 18275 (2019).
- [24] N. G. Van Kampen, The expansion of the master equation, in *Advances in Chemical Physics*, edited by I. Prigogine and S. A. Rice, 1st ed. (Wiley, New York, 1976), Vol. 34, pp. 245–309.
- [25] E. Cohen, D. A. Kessler, and H. Levine, Front propagation up a reaction rate gradient, *Phys. Rev. E* **72**, 066126 (2005).
- [26] See Supplemental Material at <http://link.aps.org/supplemental/10.1103/szpk-sx1c> for simulation details.
- [27] M. Lynch, R. Bürger, D. Butcher, and W. Gabriel, The mutational meltdown in asexual populations, *J. Hered.* **84**, 339 (1993).
- [28] H. J. Muller, The relation of recombination to mutational advance, *Mutat. Res. Fund. Mol. Mech. Mutagen.* **1**, 2 (1964).
- [29] A. Eyre-Walker and P. D. Keightley, The distribution of fitness effects of new mutations, *Nat. Rev. Genet.* **8**, 610 (2007).
- [30] M. Eigen, Self-organization of matter and the evolution of biological macromolecules, *Naturwissenschaften* **58**, 465 (1971).
- [31] J. H. Lee *et al.*, Long-primed germinal centres with enduring affinity maturation and clonal migration, *Nature (London)* **609**, 998 (2022).
- [32] P. A. Vikhar, Evolutionary algorithms: A critical review and its future prospects, in *2016 International Conference on Global Trends in Signal Processing, Information Computing and Communication (ICGTSPICC)* (IEEE, Jalgaon, India, 2016), pp. 261–265.
- [33] D. R. Mills, R. L. Peterson, and S. Spiegelman, An extracellular Darwinian experiment with a self-duplicating nucleic acid molecule, *Proc. Natl. Acad. Sci. U.S.A.* **58**, 217 (1967).

- [34] R. E. Cobb, R. Chao, and H. Zhao, Directed evolution: Past, present, and future, *AIChE J.* **59**, 1432 (2013).
- [35] X. Pan, L. Xue, Y. Lu, and N. Sun, Hybrid particle swarm optimization with simulated annealing, *Multimed. Tools Appl.* **78**, 29921 (2019).
- [36] C. Ren, X. Wen, J. Mencius, and S. Quan, Selection and screening strategies in directed evolution to improve protein stability, *Bioresour. Bioprocess.* **6**, 53 (2019).
- [37] agpyo, agpyo/mutate_PRL: mutate_PRL, 10.1103/szpk-sx1c (2025).

End Matter

Appendix: System-size expansion—The master equation corresponding to the birth-death-mutation model is

$$\frac{\partial}{\partial t} P(\vec{N}, t) = \sum_n (\hat{U}_n^{(g)} + \hat{U}_n^{(m)}) N_n P(\vec{N}, t), \quad (\text{A1})$$

where $P(\vec{N}, t)$ is the probability density corresponding to configuration $\vec{N} = [\dots, N_n, \dots]^T$. In Eq. (A1), $\hat{U}_n^{(g)}$ is the local growth operator corresponding to the birth-death process, and $\hat{U}_n^{(m)}$ is the local mutation operator. In terms of the local creation and annihilation operators $a_n^\pm f(\vec{N}) = f(\vec{N} \pm \mathbf{1}^{(n)})$, where $\mathbf{1}_m^{(n)} = \delta_{nm}$ [24], these operators are

$$\hat{U}_n^{(g)} = B_n(a_n^- - 1) + \langle B_n \rangle (a_n^+ - 1), \quad (\text{A2a})$$

$$\hat{U}_n^{(m)} = h_n^+(a_n^+ a_{n+1}^- - 1) + h_n^-(a_n^+ a_{n-1}^- - 1), \quad (\text{A2b})$$

where $h_n^+ = \gamma_b p_n B_n$ and $h_n^- = \gamma_d p_n B_n$ are, respectively, beneficial and deleterious mutation rates. Note that in Eq. (A2a), $\langle B_n \rangle$ is an average over a specific configuration \vec{N} , therefore the master equation [Eq. (A1)] is linear in $P(\vec{N}, t)$.

To perform a system-size expansion, we decompose N_n into its mean-field and noise components [24], i.e., $N_n = N\varphi_n + \sqrt{N}\xi_n$, and rewrite Eq. (A1) in terms of a probability density, $\Pi(\vec{\xi}, t)$, expressed as a function of noise configuration $\vec{\xi} = [\dots, \xi_n, \dots]^T$, i.e., $P(\vec{N}, t) \rightarrow \Pi(\vec{\xi}, t)$.

Taylor expanding the local operators and collecting like orders of system size N yields the mean-field equation [Eq. (1)]

$$\frac{\partial \varphi_n}{\partial t} = r_n \varphi_n + h_{n-1}^+ \varphi_{n-1} + h_{n+1}^- \varphi_{n+1}, \quad (\text{A3})$$

and the dynamics for the variance in the noise,

$$\begin{aligned} \frac{\partial}{\partial t} \langle \xi_n^2 \rangle_\Pi &= 2r_n \langle \xi_n^2 \rangle_\Pi + \rho_n \varphi_n \\ &+ \sum_{i \in \{-1, 1\}} h_{n-i}^i (\varphi_{n-i} + 2\langle \xi_n \xi_{n-i} \rangle_\Pi), \end{aligned} \quad (\text{A4})$$

where $\langle f_n \rangle_\Pi$ denotes average over $\Pi(\vec{\xi}, t)$. Note that by definition, $\varphi_n = 0$ for $n > n^*$. Therefore, the flux terms in Eqs. (6a) and (6b) are $J_{n^*} = p_{n^*-1} B_{n^*-1} \varphi_{n^*-1}$, and $\dot{J}_{n^*} = p_{n^*-1} B_{n^*-1} (\varphi_{n^*-1} + 2\langle \xi_{n^*} \xi_{n^*-1} \rangle_\Pi)$.